0026-895X/91/061023-6$03.00/0

MOLECULAR PHARMACOLOGY, 40:1023-1028

Molecular Mechanics and Molecular Dynamics Studies of the Intercalation of Dynemicin-A with Oligonucleotide Models of DNA

MARIO G. CARDOZO and A. J. HOPFINGER

Department of Medicinal Chemistry and Pharmacognosy, University of Illinois at Chicago, Chicago, Illinois 60680

Received April 30, 1991; Accepted September 3, 1991

SUMMARY

Intermolecular molecular modeling calculations to determine the intercalation behavior of dynemicin-A with DNA were performed using both static scanning and energy minimization and molecular dynamics relaxation techniques. Two base pair sequences, CpApCpGpGpGp-3′/GpTpGpCpCpCp-5′ and ApCpTpApCpTp-3′/TpGpApTpGpAp-5′, were considered in the calculations. The static scanning and energy minimization analyses identified multiple stable intercalation complexes for each base pair sequence. These complexes were subsequently used as starting structures in molecular dynamics relaxation simulations. Intercalation into the minor groove is preferred for both base pair sequences, and intercalation at a central CG site is preferred by about 9 kcal/mol over a TA site. However, intercalation at a TA site should be more reactive, in terms of chain scission, than that at a CG site, because dynemicin-A has more flexibility to achieve an intercalation geometry disposed to chemically react toward a base adjacent to the 3′ side of a purine. This reaction model is consistent with experimental data.

Dynemicin-A (**I**) is a novel antitumor antibiotic, isolated from *Micromonospora chersina* (1), with potent inhibitory activity against a wide range of bacteria and tumor cell lines. The chemical structure has a novel fusion of an anthraquinone ring with a tetracyclo[1,5]diyn-3-ene. The mechanism of action postulated for antitumor activity of this compound is similar to that of the esperamicins and calicheamicins families (2, 3).

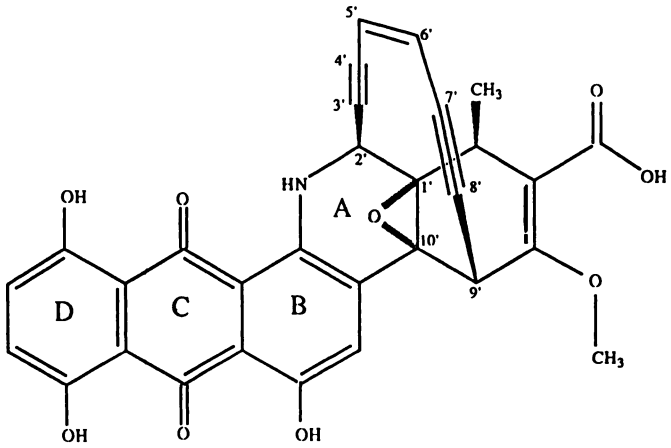

I

The 1,5-diyn-3-ene core is thought to be converted to a biradical intermediate, which is able to attack a preferred sugar of the DNA backbone. One center radical abstracts a 5′ hydrogen from the deoxyribose sugar. This reaction generates a radical species that reacts with dioxygen to form a peroxyl radical. The peroxyl radical, in the presence of thiol (RSH), then forms an aldehyde and produces DNA strand scission.

Experimental studies indicate that DNA damage is not base specific, but the attack is preferentially directed to the base adjacent to the 3′ side of a purine, with guanine a favored cutting site for dynemicin-A. The observed asymmetric cleavage pattern on the 3′ side of the complementary nucleic acid strand is consistent with the interaction of the ligand along the minor groove of DNA. In addition, pretreatment of the DNA with distamycin A and/or anthramycin significantly alters the nucleotide cleavage pattern generated by dynemicin-A. Distamycin A is a known minor groove binder, and anthramycin is a typical modifier of the guanine 2-amino group.

In contrast to other 1,5-diyn-3-ene antibiotics, the presence of an anthraquinone ring in dynemicin-A suggests a mechanism of intercalation between the base pairs similar to that observed for anthracycline antibiotics (5, 6). Still, the postulated mechanism of action involves aromatization of the 1,5-diyn-3-ene system.

Experimental results on a series of 1,5-diyn-3-ene derivatives (7) indicate that the crucial turning point from stability to spontaneous cyclization must be in the range of 3.2 to 3.3 Å between the atoms involved in the formation of the new bond ($C_{3'}$-$C_{8'}$). However, the constrained geometry of the tetracyclic structure containing the reactive 1,5-diyn-3-ene in dynemicin-

M.G.C. is a Fogarty International Fellow of the National Institutes of Health. This work was supported, in part, by the Laboratory of Computer-Aided Molecular Modeling and Design at University of Illinois at Chicago.

ABBREVIATIONS: MM, molecular mechanics; MD, molecular dynamics.

A does not permit this close approach of the reactive atoms. This distance constraint is mainly a consequence of the presence of the epoxy ring, which distorts the geometry of the attached sp^3 carbon atom ($C_{1'}$ and $C_{10'}$). As a result of this strain, the remaining atoms bonded to these carbon atoms are virtually co-planar, placing the bridge head atoms ($C_{2'}$ and $C_{9'}$) in a rigid and quasiplanar *trans*-conformation. This constrained geometry, in turn, limits the positions and motions of the reactive atoms and prevents their reaction. Therefore, hydrolysis of the epoxy ring is required in order to relax the strain of the 1,5-diyn-3-ene unit included in the 10-member ring and to bring the reactive centers close enough for spontaneous cyclization.

We have focused upon identifying the preferred geometry of the intercalation complex and how these geometries might favor both the intra- and intermolecular reactions involved in the postulated action mechanism. The results presented here were obtained using both static and dynamic MM methods.

Procedures and Results

Intramolecular structures. The geometry of dynemicin-A used in this study was obtained by energy minimization of a trial structure using the quantum mechanical method MOPAC (8) and the MM method MMFF of CHEMLAB-II (9, 10). The conformations of the methoxy and carboxilic acid substituents were obtained from a fixed valence conformational energy scan at 10° increments about their principal bonds (11). The dihedral angles of the methoxy and carbonyl groups, with respect to the vinyl double bond, are 212° and 177°, respectively.

CTAC-3′ and ACGG-3′ tetramers and ACTACT-3′ and CACGGG-3′ hexamer sequence duplexes were used to model DNA macromolecules. The central base pair was initially assigned the crystal geometry of the CpGp-3′/CpGp-5′-ethidium ion complex (12). The TA central dimer sequence was built using the backbone geometry of the CG-3′-ethidium ion complex and the X-ray crystal structure of the corresponding thymine and adenine bases. The remaining base pairs were added above and below the central dimer so as to mimic the B-form DNA conformation (13). The resulting initial geometries were then optimized in MMFF, using an AMBER-modified force field (14) and CNDO/2 charges (15) for the ionic state, with the constraint that the center two base pairs remained positioned at the observed intercalation separation distance.

Static intermolecular modeling. Fixed valence geometry intermolecular energy scans were first performed using the minimum energy geometry of dynemicin-A and the ApCpGpGp-3′/TpGpCpCp-5′ and CpTpApCp-3′/GpApTpGp-5′ tetramers with an open central base pair structure. The ligand-DNA intermolecular energy was scanned over a three-dimensional grid of points, holding the DNA tetramer conformation rigid. Each grid of points can be specified using the six degrees of freedom defined by Hopfinger and co-workers (16) and shown in Fig. 1. In addition, the positions of the hydroxyl groups in dynemicin-A were fixed to several planar conformations, which pointed toward and away from the carbonyl groups for each intermolecular energy scan. A nonbonded MM force field, composed of dispersion/steric, electrostatic, and hydrogen bond contributions, was used to determine the energy at each grid point. The nonbonded AMBER-CLONE parameters were used to compute the dispersion/steric atom-pair interactions (14). The electrostatic interactions were calculated using a coulombic representation with the molecular dielectric constant

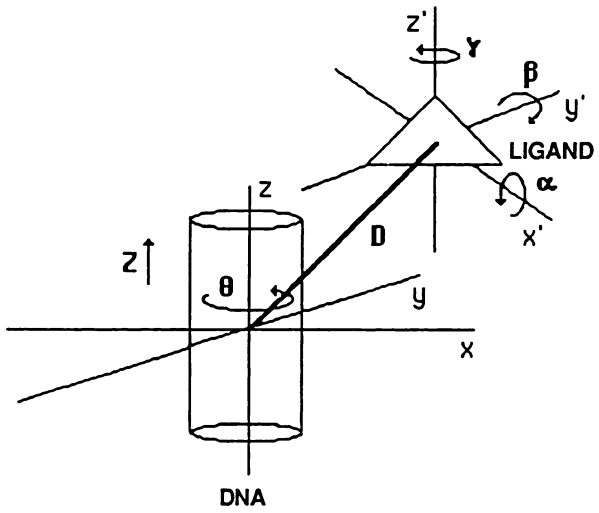

Fig. 1. Intermolecular fixed valence geometry degrees of freedom used to scan about the DNA model (*cylinder*) by the ligand (*triangle*).

equal to 3.5 and atomic charges calculated by the CNDO/2 method (15). Each apparent intermolecular minimum energy state identified in the scan was used as a starting point for a fixed valence geometry energy minimization with respect to the six intermolecular degrees of freedom. Table 1 contains the results of these calculations.

Figs. 2 and 3 show the global minimum energy intermolecular geometries for the intercalation of dynemicin-A and the two DNA model tetramers, based upon the fixed valence geometry static calculations. For both sequences studied, intercalation into the minor groove is favored by about 8 kcal/mol, compared with the major groove. For each groove two different intercalation complexes are found, which have the 1,5-diyn-3-ene bridge oriented in opposite directions to the "top" (U and U′) and "bottom" (D and D′) of the DNA helical axis. The intercalation of the anthraquinone ring is, in most cases, perpendicular to the base pair axes. The perpendicular orientation of the 1,5-diyn-3-ene bridge with respect to the anthraquinone portion regulates the depth of intercalation of the anthraquinone moiety between the two center base pairs. In contrast to intercalation of daunomycin, the corresponding D-ring in dynemicin-A overlaps completely with the adjacent base pairs in the intercalation site. This overlap leads to favorable charge-charge interactions between the phenol hydroxyl group and oxygen atoms of the phosphate groups, in addition to the dispersion and complementary electrostatic interactions of the anthraquinone ring with the adjacent base pairs.

The gain in stabilization intermolecular energy for preferential intercalation into the minor groove, compared with the major groove, is due to a favorable geometry for charge-charge interactions for the minor groove (see Figs. 2 and 3). In the case of minor groove intercalation, the anthraquinone ring is perpendicular to the adjacent base pairs, with attractive charge-charge interactions between a hydroxyl proton of the D-ring of dynemicin-A and an oxygen of the phosphate group, the hydroxyl proton of the B-ring and the oxygen of one deoxyribose sugar, and the hydrogen of the secondary amine and the oxygen of the other deoxyribose sugar of the central base pairs.

Intercalation into the major groove, for the CG-3′ central base pair model, shows two different stable geometries. In one case, intercalation of the anthraquinone ring is perpendicular to adjacent base pairs, and there are only two favorable charge-

TABLE 1

Results of the static MM calculations. Summary of the location (see Fig. 1) and relative energies of the minimum energy complexes for a $(ACGG)_2$ tetramer and dynemicin-A (A) or a $(CTAC)_2$ tetramer and dynemicin-A (B). ΔE refers to the DNA-ligand interaction energy. The energies are referenced to the most stable structure as zero

	Minimum	α	β	γ	θ	Z	d	ΔE	Groove
						Å	Å	kcal/mol	
A.	1U	−4.8°	179.1°	94.3°	64.0°	0.06	2.56	0.0	Minor
	2U	−1.4	177.8	111.9	286.6	−0.08	2.41	8.1	Major
	1D	8.7	−5.8	116.9	214.7	0.14	−3.37	1.9	Minor
	2D	−3.3	−4.7	123.1	14.4	0.19	−1.55	11.3	Major
B.	1U′	−3.8	179.0	99.7	66.9	−0.02	2.42	0.0	Minor
	2U′	−4.6	178.2	112.8	284.9	0.06	2.93	8.8	Major
	1D′	8.6	0.6	107.2	7.8	−0.17	−2.24	9.5	Major
	2D′	11.5	−5.8	99.7	209.6	0.30	−6.07	28.0	Minor

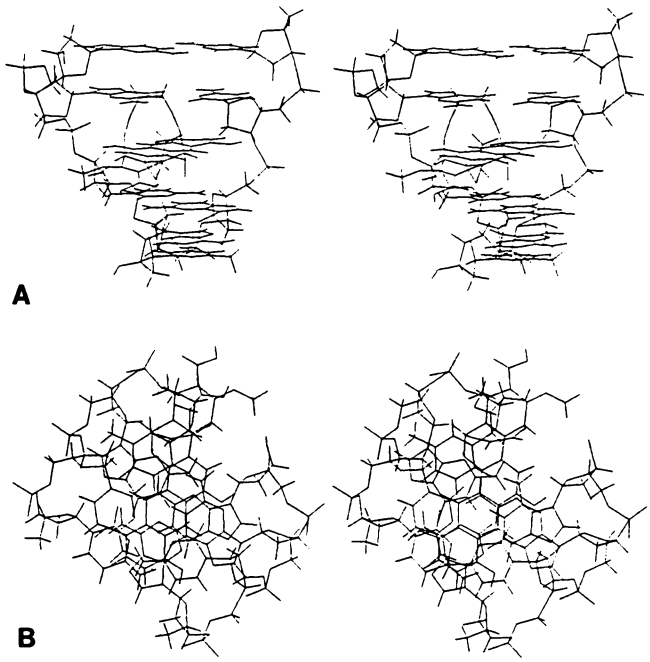

Fig. 2. Apparent global minimum energy intercalation geometry for dynemicin-A with the ApCpGpGp-3′/TpGpCpCp-5′ duplex, 1U, using a fixed valence geometry scan of intermolecular space. A, Side view from the minor groove; B, top view.

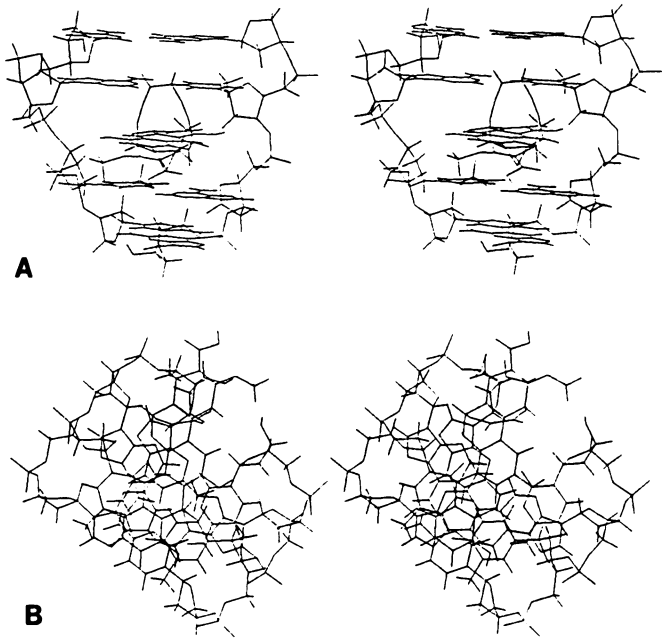

Fig. 3. Same as Fig. 2, but for the dynemicin-A-CpTpApCp-3′/GpAp-TpGp-5′ duplex in the 1U′ intercalation complex.

charge interactions between the protons of the hydroxyl groups of the D- and B-rings and the nearest oxygen atoms of the deoxyribose sugars. In the other major groove intercalation geometry, the anthraquinone ring is displaced 30° from being perpendicular. No favorable charge-charge interactions occur. In addition, the displacement from perpendicular intercalation diminishes dispersion interactions between the anthraquinone ring and the adjacent base pairs.

Both major groove intercalation geometries, for the TA-3′ base pair sequence, have the anthraquinone ring displaced from being perpendicular to the base pair axis. These higher energy intercalation complexes are stabilized by the same intermolecular energy interactions described for the CG-3′ major groove intercalation geometries.

MD. We performed MD simulations using all of the intermolecular minimum energy geometries found in the static MM studies as initial MD states. The MOLSIM MD package (17) was used in all MD simulations. For these calculations, the hexamer duplex structures for CpApCpGpGpGp-3′/GpTpGpCpCpCp-5′ and ApCpTpApCpTp-3′/TpGpApGpAp-5′ were used to model DNA. MD is useful in generating a relaxed representation of molecular structure with respect to both nonbonded and valence geometry interactions. We find that the low energy structures on the MD trajectories are virtually identical in geometry and energy to the corresponding fully optimized intercalation complexes. MD simulation is also a convenient method to use to isolate and study the motion of the 1,5-diyn-3-ene bridge. As mentioned, this bridge appears to play an important role in the determination of the intercalation geometry of the anthraquinone ring, due to repulsive steric forces between its atoms and those of the adjacent base pairs. MD simulation might indicate some relaxation of these repulsive interactions, giving a different "picture" of the intermolecular complex than that found by the more rigid static energy minimization.

The MD equilibration of each starting interaction geometry was performed using the method developed by Kawakami and Hopfinger.[1] This equilibration process is a combination of enhanced atomic mass treatment and temperature variation, in order to simulate an infinite DNA polymer and to relax the central base pair-ligand interaction geometry. In addition, torsion angle restrictions for each of the dihedral angles O-C1′-

[1] Y. Kawakami and A. J. Hopfinger, manuscript in preparation.

N1-C2 of the end base pairs were added to the original force field parameters. This restriction was implemented in order to damp rotation and bending of the ends of the oligonucleotide model. The torsion potential function used has equal minimum values corresponding to the base pair geometry of B-form DNA and maximum values for base pair geometries perpendicular to the minima. A value of 15 kcal/mol was assigned to the torsion barrier height to minimize nonplanar motions.

After equilibration, 10-psec MD simulation at 100°K was performed using the same mass treatment and torsion angle restrictions as used in the equilibration phase. The MM force field was the same as in the static energy minimization study (the AMBER valence geometry contribution was also included). The lowest energy complex of the trajectory was taken as the most representative intercalation geometry for each series of MD simulations. Table 2 contains the lowest ligand-DNA intermolecular energies obtained from the MD trajectories. The differences in energy, ΔE, represent the relative stability of each complex with respect to the lowest energy intercalation complex observed on the trajectory.

As in the static study, intercalation into the minor groove is more stable than that of the major groove. However, the difference in energy found is reduced to only 6.2 and 4.0 kcal/mol between the lowest energy major and minor groove complexes for the CG-3′ and TA-3′ intercalation complexes, respectively. In general, the difference in stability is mainly due to a larger attractive contribution in intermolecular dispersion energy for the minor groove.

A comparison of the relative stabilities of the intercalation complexes in Tables 1 and 2 indicates that the MD simulation can relax geometries of a complex to such an extent, relative to fixed-geometry static energy minimizations, that there are changes in relative complex stability. The 1D structure of Table 1A goes from being 1.9 kcal/mol less stable than structure 1U to being 3.5 kcal/mol more stable than 1U upon MD relaxation. Likewise, structure 2D′ goes from being 28.0 kcal/mol less stable than 1U to being 2.8 kcal/mol more stable, being now the MD apparent global minimum intermolecular energy complex for the TA-3′ intercalation complex.

In addition, the MD low-energy intercalation geometry, for each sequence studied, has the 1,5-diyn-3-ene bridge oriented toward the "bottom" of the DNA helical axis, which is opposite to the geometry of the minima found in the static calculations.

TABLE 2

Results of the MD calculations. Summary of the MD low energy structures of a $(CACGGG)_2$ hexamer and dynemicin-A (A) or a $(ACTACT)_2$ hexamer and dynemicin-A (B). E_c is the ligand-DNA coulombic energy, E_{vdw} is the ligand-DNA van der Waals energy, and ΔE is the intercalation energy relative to the lowest energy complex, having $\Delta E = 0$

	Starting point*	Energy				
		E_c	E_{vdw}	$(E_c + E_{vdw}) = E$	ΔE	Groove
		kcal/mol				
A.	1U	−15.3	−57.7	−73.0	3.5	Minor
	2U	−10.9	−57.2	−68.1	8.4	Major
	1D	−18.1	−58.4	−76.5	0.0	Minor
	2D	−13.3	−57.0	−70.3	6.2	Major
B.	1U′	−8.9	−56.0	−64.9	2.8	Minor
	2U′	−13.2	−50.5	−63.7	4.0	Major
	1D′	−15.4	−45.5	−60.9	6.8	Major
	2D′	−14.3	−53.4	−67.7	0.0	Minor

* The apparent energy minima reported in Table 1 were used as the starting points.

Figs. 4 and 5 represent the 1D and 2D′ relaxed (low-energy) intercalation complexes.

Overall, for both sequences studied, MD simulations indicate that minor groove intercalation of dynemicin-A is energetically preferred to major groove entry into DNA.

Discussion

A comparison of the E_c and E_{vdw} values in Table 2 indicates that the attractive dispersion and coulombic interactions are

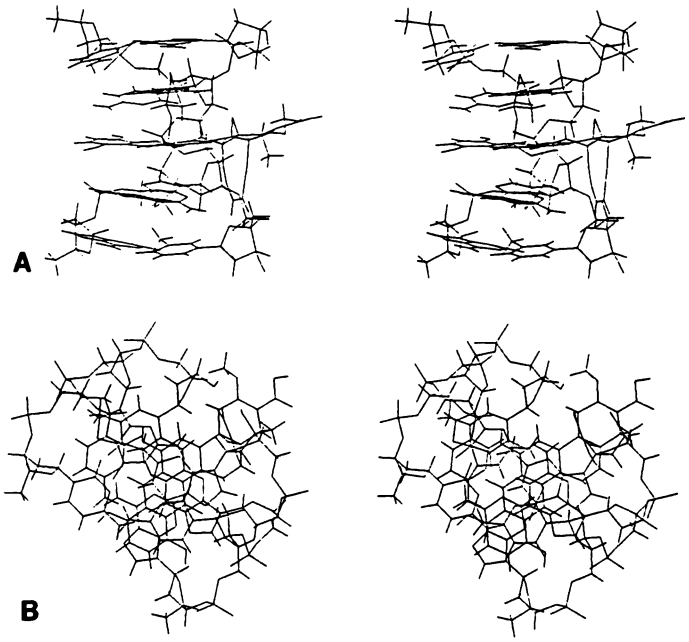

Fig. 4. Low-energy intercalation complex for dynemicin-A with the Cp-ApCpGpGpGp-3′/GpTpGpCpCpCp-5′ duplex, 1D, using MD. A, Side view from the ACGG-3′ strand; B, top view.

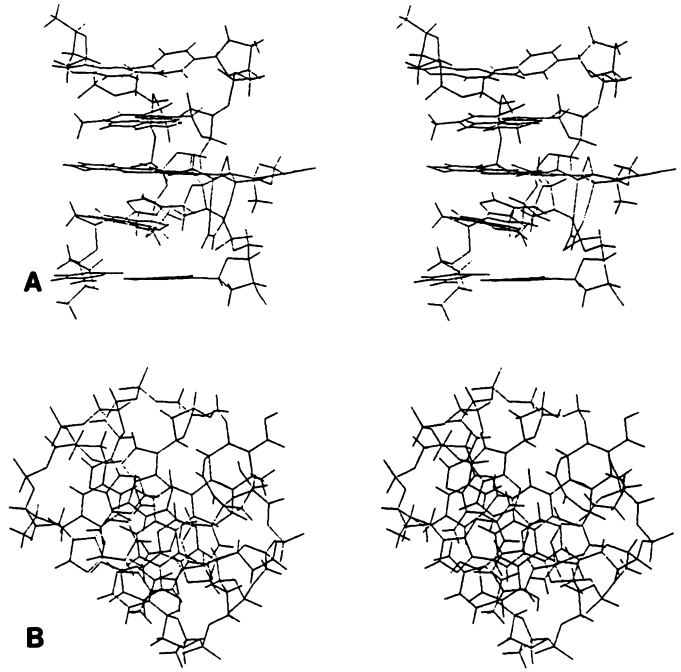

Fig. 5. Same as Fig. 4, but for the dynemicin-A-ApCpTpApCpTp-3′/TpGpApTpGpAp-5′ duplex in the 2D′ intercalation complex. A, Side view from the CTAC-3′; B, top view.

the principal sources of stabilization for the intercalation complex. As observed in our other ligand-DNA intercalation modeling studies (18, 19), there are multiple minimum energy intercalation structures. Intercalation energy minima up to 10 kcal/mol above the global free space minimum have been retained as possible structures, because solvation energetics have been neglected. Simple aqueous hydration-shell solvation modeling calculations (20) suggest that different intercalation geometries, for the same ligand-DNA model, can vary in solvation energy up to 7 kcal/mol/complex.

The results of the MD versus static minimization calculations suggest that the fixed valence geometry approximation introduces unrealistic rigidity into structures being considered in intermolecular modeling. As such, the relative stabilities of corresponding minimum energy complexes may be in serious error. On the other hand, the fixed valence geometry approximation does seem to be a useful and efficient means of exploring for proximate intermolecular geometries to use as starting points in MD relaxation studies.

Inspection of the MD trajectories suggests that a favorable ligand-DNA reaction geometry involving the 1,5-diyn-3-ene core is possible for intercalation of dynemicin-A into the minor groove. On the other hand, intercalation into the major groove yields a complex in which the postulated reactive center of dynemicin-A not only is far from the reactive 5′-methylene of the DNA but also is in an unfavorable steric geometry. Therefore, the four minor groove intercalation complexes, two for each sequence studied, can be considered as suitable geometries for the intramolecular cyclization of the ligand and its subsequent reaction with DNA. Fig. 6 provides a schematic representation of these four intercalation geometries and indicates the postulated ligand-DNA reaction sites.

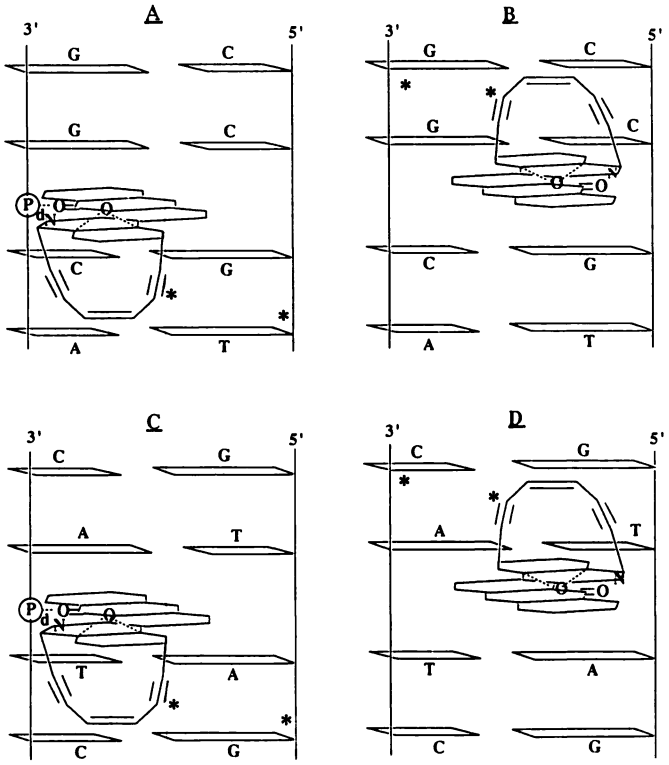

Fig. 6. Schematic representation of the four minor groove intercalation geometries favoring direct ligand-DNA reactions. A, 1D; B, 1U; C, 2D′; D, 1U′. *d*, Interatomic distance between the DNA chain phosphorus and the carbonyl oxygen of dynemicin-A.

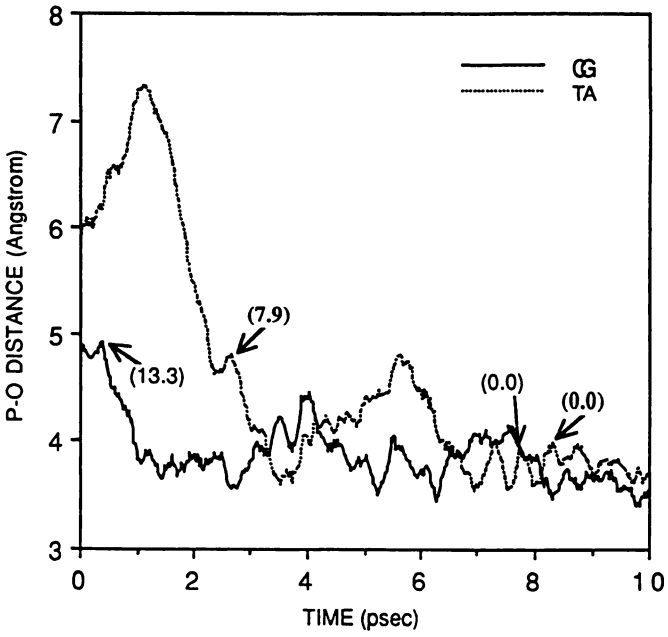

Fig. 7. Trajectory plot of the interatomic distance between the phosphorus atom of the central base pairs of the 3′ strand (opposite to the reactive strand) and the carbonyl oxygen atom of dynemicin-A, for the 1D-CG and the 2D′-TA intercalation states, as a function of time. *Numbers in parentheses*, increase in intercalation energy with respect to each of the two global minima (0.0), corresponding to increasing the interatomic distance, P···O, 1 Å.

Both MD global low-energy intercalation geometries, 1D and 2D′ (see Table 2), have the anthraquinone ring intercalated in the space between the central base pairs of the 3′ strand. In order to minimize steric repulsions between the 1,5-dyin-3-ene ring and the adjacent base pairs, the intercalation of the anthraquinone moiety is approximately diagonal with respect to the two base pair axes and the D-ring is close to the sugar phosphate backbone. A similar situation occurs for both of the local minimum energy intercalation complexes, 1U and 1U′, but in these structures the anthraquinone is displaced in the direction of the 5′ strand (see Fig. 6).

A comparison of the intermolecular ligand-DNA energies for the global low energy structures reported in Table 2 shows an intercalation preference of about 9 kcal/mol for the CG-3′ central base pairs, compared with TA-3′. This difference in energy is mainly due to a stronger dispersion attraction between the anthraquinone moiety and the adjacent CG bases than the TA bases. Ornstein and Rein (21) and Miller and Pycior (22) have each computed that the opening of the DNA chain from the B-form to the intercalation geometry requires about 1 kcal/mol less energy when one of the central base pairs is CG-3′, as opposed to AT-3′. This process would additionally favor intercalation at the CG-3 site. However, experimental results (4) indicate that intercalation into the TpAp-3′/ApTp-5′ region yields major DNA chain scission. This cutting occurs at a 5′-methylene between the AG bases of the sequence CpTpApCp-3′/GpApTpGp-5′.

At this point, it is not clear why the TA region is more reactive, compared with the CG site. The lowest energy intercalation complexes for both sequences have the ligand located in a space opposite to the strand containing the DNA reactive site. In order to bring the reactive center of the ligand close enough for a reaction, both intercalation complexes need to alter the preferred positions of the bound dynemicin-A, after

its conversion to the diaryl radical form, which is the DNA-cleaving intermediate. Thus, relative changes in ligand-DNA interaction energy, for a given intercalation state and sequence binding site, may play an important role in determining the relative reactivity of dynemicin-A at relative sequence sites, because these interactions control the thermodynamic propensity to change intercalation geometries to, in turn, realize a reaction process.

Dynemicin-A-DNA intermolecular energy explorations indicate that, for TA-3′ intercalation, dynemicin-A has a weaker intermolecular attraction for the strand opposite that of the DNA reactive site, compared with CG-3′ intercalation. Thus, this weaker intermolecular attraction in the TA-3′ intercalation site is expected to more easily permit the displacement of the ligand, inside the intercalation site, in the direction of the reactive DNA strand, compared with the CG-3′ "receptor" site. The displacement of dynemicin-A from the TA-3′ minimum energy intercalation state to another state, closer to the reactive DNA strand, does, in fact, require less energy than for equivalent geometric changes associated with CG-3′ intercalation. Fig. 7 is a trajectory plot of the interatomic distance between the phosphorus atom of the central base pairs of the 3′ strand (refer to Fig. 6), and the carbonyl oxygen atom of dynemicin-A, for both CG and TA intercalation sites. The MD simulation results indicate that for the CG intercalation site 13.3 kcal/mol is required to move the ligand 1 Å in the direction of the reactive strand from the minimum energy intercalation position. An equivalent displacement requires only 7.9 kcal/mol for the TA-3′ intercalation site. This site-specific energy relationship is expected to be conserved over the course of the reaction, because the structural changes in the reacting ligand, after cyclization of the 1,5-diyn-3-ene ring, will be the same for both intercalation complexes. In addition, these changes exhibit very minimal modifications to the electronic and molecular shape properties of the anthaquinone moiety, which are mainly responsible for intercalation energetics and geometry.

Our explanation of the observed base sequence reaction specificity for the chain-cutting action of dynemicin-A does not include the calculated intercalation energy preference for a CG-3′ site. Our modeling indicates that the intercalation of dynemicin-A at the CG-3′ site is about 9 kcal/mol more stable than intercalation at the TA-3′ site. This implies a major discrepancy with experimental chain scission behavior if one assumes that equilibrium binding thermodynamics govern the chemical reaction processes. Our findings suggest that equilibrium intercalation binding states may not be involved in the reactions leading to chain scissions. Instead, reaction may occur at short time intervals after intercalation, compared with the resident times of intercalation for both CG-3′ and TA-3′ sites. In this way the concentration component to reactivity, which favors action with CG-3′ base pairs because they are part of the preferred binding sites, is not operative. Further, a dynemicin-A molecule should have about equal chances of approaching the DNA at CG or TA locations, because the "surface" of the biopolymer is largely that of the sugar phosphate chains.

Of course, TA-3′ specificity could also arise from conformational changes in the DNA due to intercalation at one site that predisposes a nearby TA-3′ site to be highly favorable. Such intricate and coupled intercalation systems are very difficult to model. Our next study will, instead, consider the proposed chemical reaction pathways of the DNA-dynemicin-A interaction.

Acknowledgments

We very much appreciate the help of Dr. Y. Kawakami, on leave from Eisai Research Laboratories, Tsukuba, Japan, during the course of part of this investigation.

References

1. Konishi, M., H. Ohkuma, K. Matsumoto, T. Tsumo, H. Kamei, T. Miyaki, T. Oki, H. Kawaguchi, G. D. Van Duyne, and J. Clardy. Dynemicin A, a novel antibiotic with the anthraquinone and 1,5-diyn-3-ene subunit. *J. Antibiot. (Tokyo)* **42**:1449–1452 (1989).
2. Long, B. H., J. Golik, S. Forenza, B. Ward, R. Rehfuss, J. Dabrowiak, J. Catino, S. T. Musial, K. W. Brookshire, and T. W. Doyle. Esperamicins, a class of potent antitumor antibiotics: mechanism of action. *Proc. Natl. Acad. Sci. USA* **86**:2–6 (1989).
3. Zein, M., A. M. Sinha, W. J. McGahren, and G. A. Ellestad. Calicheamicin $\gamma 1^I$: an antitumor antibiotic that cleaves double-stranded DNA site specifically. *Science* (Washington D. C.) **240**:1198–1201 (1988).
4. Sugiura, Y., T. Shiraki, M. Konishi, and T. Oki. DNA intercalation and cleavage of an antitumor antibiotic dynemicin that contains anthracycline and enediyne cores. *Proc. Natl. Acad. Sci. USA* **87**:3831–3835 (1990).
5. Quigley, G. J., A. H.-J. Wang, G. Ughetto, G. van der Marel, J. H. van Boom, and A. Rich. Molecular structure of an anticancer drug-DNA complex: daunomycin plus d(CpGpTpApCpG). *Proc. Natl. Acad. Sci. USA* **77**:7204–7208 (1980).
6. Patel, D. J., S. A. Kozlowski, and J. A. Rice. Hydrogen bonding, overlap geometry, and sequence specificity in anthracycline antitumor antibiotic-DNA complexes in solution. *Proc. Natl. Acad. Sci. USA* **78**:3333–3337 (1981).
7. Nicolaou, K. C., G. Zucarello, Y. Ogawa, E. J. Schweiger, and T. Kumazawa. Cyclic conjugated enediynes related to calicheamicins and esperamicin: calculations, synthesis, and properties. *J. Am. Chem. Soc.* **110**:4866–4868 (1988).
8. Steward, J. J. P., and F. K. Seiler. MOPAC: a general molecular orbital package (version 5.0). *QCPE Bull.* 455 (1988).
9. Allinger, N. L. Conformational analysis. 130. MM2: a hydrocarbon force field utilizing V_1 and V_2 torsional terms. *J. Am. Chem. Soc.* **99**:8127–8133 (1977).
10. CHEMLAB-II (version 11.0) Molecular Design Ltd., San Leandro, CA (1991).
11. Hopfinger, A. J. *Conformational Properties of Macromolecules*. Academic Press, New York (1973).
12. Jain, S. C., C.-C. Tsai, and H. M. Sobell. Visualization of drug-nucleic acid interactions at atomic resolution. II. Structure of an ethidium/dinucleotide monophosphate crystalline complex, ethidium:5-iodocytidylyl(3′-5′)guanosine. *J. Mol. Biol.* **114**:317–331 (1977).
13. Arnot, S., P. J. Campbell-Smith, and H. Chandrasekaran. *Handbook of Biochemistry and Molecular Biology, Nucleic Acid* (O. D. Fasman, ed.), Vol. 2. CRC Press, Cleveland, OH, 137 (1976).
14. Weiner, S. J. A new force field for molecular mechanical simulation of nucleic acid and protein. *J. Am. Chem. Soc.* **106**:765–777 (1984).
15. Pople, J. A., and D. C. Beveridge. *Approximate Molecular Orbital Theory*. McGraw-Hill, New York (1970).
16. Malhotra, D., R. Pearlstein, O. Kikuchi, Y. Nakata, and A. J. Hopfinger. Alkylation, intercalation, and conformational properties of nucleic acid structures. *Ann. N. Y. Acad. Sci.* **367**:295–325 (1981).
17. Doherty, D. C., and A. J. Hopfinger. Molecular modeling of polymers. 6. Intramolecular conformational analyses and molecular modeling of syndiotactic polystyrene. *Macromolecules* **22**:2472–2477 (1989).
18. Kikuchi, O., R. Pearlstein, A. J. Hopfinger, and D. R. Bickers. Transition-state alkylation geometries of 7,8-dihydroxy-9,10-epoxy-7,8,9,10-tetrahydrobenzo[*a*]pyrene: enantiomeric isomers with nucleic acid dimers. *J. Pharm. Sci.* **72**:800–808 (1983).
19. Nakata, Y., and A. J. Hopfinger. Predicted mode of intercalation of doxorubicin with dinucleotide dimers. *Biochem. Biophys. Res. Commun.* **95**:583–588 (1980).
20. Malhotra, D., and A. J. Hopfinger. Conformational flexibility of dinucleotide dimers during unwinding from B-form to an intercalation structure. *Nucleic Acids Res.* **8**:5289–5304 (1980).
21. Ornstein, R. L., and R. Rein. Energetics of intercalation specificity. I. Backbone unwinding. *Biopolymers* **18**:1277–1291 (1979).
22. Miller, K. J., and J. F. Pycior. Interaction of molecules with nucleic acids. II. Two pairs of families of intercalation sites, unwinding angles, and the neighbor-exclusion principle. *Biopolymers* **8**:2683–2719 (1979).

Send reprint requests to: A. J. Hopfinger, Department of Medicinal Chemistry and Pharmacognosy, M/C 781, University of Illinois at Chicago, Box 6998, Chicago, IL 60680.